The Utility of Modeling and Simulation in Determining Transport Performance Properties of Semiconductors

Bernardo Cockburn[1], Joseph W. Jerome[2], and Chi-Wang Shu[3]

[1] Department of Mathematics, University of Minnesota, Minneapolis, MN 55455
[2] Department of Mathematics, Northwestern University, Evanston, IL 60208
[3] Division of Applied Mathematics, Brown University, Providence, RI 02912

Abstract. The RKDG method has been effectively used in modeling and simulating semiconductor devices, where the underlying models are hydrodynamic in nature. These include classical as well as quantum models. In this paper, we survey and interpret some of these results. For classical transport, we review the simulation of a benchmark MESFET transistor by means of discontinuous Galerkin methods of degree one. For quantum transport, we report the success in simulation of the resonant tunneling diode. The principal features here are negative differential resistance and hysteresis.

1 Introduction

The goal of this work is to survey the effectiveness of continuum (hydrodynamic) models in one and two dimensions via discontinuous Galerkin methods, which were effectively used in [4] and in [5] for classical and quantum models, respectively. We choose for the underlying classical application that of charge transport in a MESFET transistor. This is a benchmark which has been studied intensively, and thus its characteristics are reliably determined (see [10,11,4,3]). For the quantum application, we select another benchmark, the resonant tunneling diode. For this device, Gardner developed a quantum hydrodynamic model in [8] (consult also for relevant references in the physics and device literature). Important characteristics of the hydrodynamic model include heat conduction, relaxation, and electrical forcing and heating terms. In particular, carrier transport occurs in a self-consistent electric field. The model is decidedly more complex than the standard gas dynamics model. The quantum model (QHD) includes perturbation terms in the pressure tensor and energy expression. These are characterized in the QHD model as third order derivative perturbations of the concentrations.

2 The Classical Hydrodynamic Model

The hydrodynamic model may be described as in [2,4]. A derivation is provided in [9] and an existence theorem for the reduced, two-carrier model is

given in [3]. It may be characterized as a second-order perturbation of a nonlinear hyperbolic system for n, the electron density, $\mathbf{p}$, the momentum density, and w, the energy density,

$$\partial_t n + \nabla \cdot (n\mathbf{v}) = 0, \tag{1}$$

$$\partial_t \mathbf{p} + \mathbf{v}\nabla \cdot \mathbf{p} + \mathbf{p} \cdot \nabla \mathbf{v} + \nabla(knT) = -en\mathbf{E} + (\partial_t \mathbf{p})_c, \tag{2}$$

$$\partial_t w + \nabla \cdot (\mathbf{v}w) + \nabla \cdot (\mathbf{v}knT + \mathbf{q}) = -en\mathbf{v} \cdot \mathbf{E} + (\partial_t w)_c, \tag{3}$$

where k is Boltzmann's constant and the velocity $\mathbf{v}$, the temperature T, and the heat flux $\mathbf{q}$ are given by

$$\mathbf{p} = mn\mathbf{v}, \tag{4}$$

$$w = \tfrac{3}{2}knT + \tfrac{1}{2}mn|\mathbf{v}|^2, \tag{5}$$

$$\mathbf{q} = -\nabla \cdot (\kappa \nabla \mathbf{T}), \tag{6}$$

where m is the effective electron mass. These equations are coupled with a Poisson equation defining the electric field $\mathbf{E}$:

$$\mathbf{E} = -\nabla \phi, \tag{7}$$

$$\nabla \cdot (\epsilon \nabla \phi) = -e (n_d - n), \tag{8}$$

where ϵ is the dielectric constant, and n_d is the doping density. The constant $e > 0$ is the electronic charge and κ is the heat conduction coefficient. The 'collision' terms are obtained by defining the momentum and energy relaxation times, $\tau_{\mathbf{p}}$ and τ_w, following [1] as

$$(\partial_t \mathbf{p})_c = -\frac{\mathbf{p}}{\tau_{\mathbf{p}}}, \qquad \tau_{\mathbf{p}} = m\frac{\mu_{n0}}{e}\frac{T_0}{T}, \tag{9}$$

$$(\partial_t w)_c = -\frac{w - \tfrac{3}{2}nT_0}{\tau_w}, \qquad \tau_w = \frac{\tau_{\mathbf{p}}}{2} + \frac{3}{2}\frac{\mu_{n0}}{ev_s^2}\frac{kTT_0}{T + T_0}, \tag{10}$$

where T_0 is the ambient temperature, $\mu_{n0} = \mu_{n0}(T_0, n_d)$ is the low field electron mobility, and $v_s = v_s(T_0)$ is the saturation velocity. Finally, κ is determined by the Wiedemann-Franz law

$$\kappa = \kappa_0 \frac{\mu_{n0}}{e} k^2 nT \left(\frac{T}{T_0}\right)^r.$$

In this paper, we take $r = -1$. We have selected a MESFET because of its acknowledged importance, particularly in microwave applications. It represents an application for which numerical methods are required to be robust over a wide parameter regime, although in this paper we restrict attention to ambient room temperature. We emphasize the importance of retention of the convective term, $\mathbf{p} \cdot \nabla \mathbf{v}$, in (2), if a robust model is desired. This is the term which permits shocks in the hydrodynamic model when present.

3 Numerical Method

3.1 General Description

To describe our numerical method, we first write the initial boundary value problem for $\mathbf{u} = (n, p_x, p_y, w)^t$ as follows:

$$\partial_t \mathbf{u} + \nabla \cdot \mathbf{F}(\mathbf{u}) = \mathbf{R}(\mathbf{u}), \qquad \text{in } (0, t_f) \times \Omega, \tag{11}$$

$$\mathbf{u}(t = 0) = \mathbf{u}_0, \qquad \text{on } \Omega, \tag{12}$$

$$\mathbf{B}\mathbf{u} = \mathbf{g}, \qquad \text{on } (0, t_f) \times \partial\Omega, \tag{13}$$

where the flux $\mathbf{F} = (\mathbf{f}_x, \mathbf{f}_y)$ has the following components:

$$\mathbf{f}_x(\mathbf{u}) = v_x \mathbf{u} + (0, nT, 0, v_x nT)^t, \tag{14}$$

$$\mathbf{f}_y(\mathbf{u}) = v_y \mathbf{u} + (0, 0, nT, v_y nT)^t, \tag{15}$$

the right-hand side $\mathbf{R}$ is given by

$$\mathbf{R}(\mathbf{u}) = \xi_{\mathbf{E}}(\mathbf{u}) + \xi_c(\mathbf{u}) + \xi_{heat}(\mathbf{u}), \tag{16}$$

$$\xi_{\mathbf{E}}(\mathbf{u}) = (0, -e\,n\,E_x, -e\,n\,E_y, -e\,n\,\mathbf{v} \cdot \mathbf{E})^t, \tag{17}$$

$$\xi_c(\mathbf{u}) = \left(0, (\partial_t p_x)_c, (\partial_t p_y)_c, (\partial_t w)_c\right)^t, \tag{18}$$

$$\xi_{heat}(\mathbf{u}) = (0, 0, 0, \nabla \cdot (\kappa \nabla T))^t, \tag{19}$$

and $\mathbf{B}$ is a matrix-valued function.

An overview of the discretization of our equations is as follows. First, we triangulate our domain Ω with triangulations $\mathcal{T}_h$ made solely of rectangles R such that the intersection of two distinct rectangles of the triangulation $\mathcal{T}_h$ is either an edge, a vertex, or void. Then, for each $t \in (0, t_f]$, we take each of the components of our approximate solution $\mathbf{u}_h(t)$ in the space

$$V_h = \{p \in L^\infty(\Omega) : \ p|_R \text{ is linear}, \forall R \in \mathcal{T}_h\}. \tag{20}$$

We define each of the components of $\mathbf{u}_{0h}$ to be the L^2-projection of the corresponding component of $\mathbf{u}_0$ into V_h and discretize the equation (11) in space by using the Discontinuous Galerkin (DG) method. Since the functions of the space V_h are discontinuous, the mass matrix of the DG method is block-diagonal. Thus, the resulting discrete equations can be rewritten as the following ODE initial value problem:

$$\frac{d\mathbf{u}_h}{dt} = \mathbf{L}_h(\mathbf{u}_h, \mathbf{g}) + \mathbf{R}_h(\mathbf{u}_h), \quad t \in (0, t_f], \tag{21}$$

$$\mathbf{u}_h(t = 0) = \mathbf{u}_{0h}, \tag{22}$$

where $\mathbf{L}_h$ is the approximation of $-\nabla \cdot \mathbf{F}$. The exact solution of the above initial value problem gives an approximation which is formally second-order accurate in space; see [6]. Accordingly, a second-order accurate in time Runge-Kutta method must be used to discretize our ODE; see [6], [13], and [14]. Finally, a local projection $\Lambda \Pi_h$ is applied to the intermediate values of the Runge-Kutta discretization in order to enforce nonlinear stability. We give a short description of several components of the algorithm below but refer the reader to the cited papers for more details.

3.2 The Discontinuous Galerkin method

The general definition of the DG method in the case of a scalar $\mathbf{u}$ can be found in [6]. To define the method in our case, we simply have to apply the procedure for the scalar case component by component.

Let us denote by $\mathbf{u}^{\{k\}}$ the k-th component of the vector $\mathbf{u}$. Consider the equation for the k-th component of the system (11), multiply it by $v_h \in V_h$, integrate over each $R \in \mathcal{T}_h$, replace the exact solution $\mathbf{u}$ by its approximation $\mathbf{u}_h$, and formally integrate by parts to obtain

$$\frac{d}{dt} \int_R \mathbf{u}_h^{\{k\}}(t,x,y)\, v_h(x,y) dx\, dy$$

$$+ \sum_{e \in \partial R} \int_e \mathbf{F}^{\{k\}}(\mathbf{u}_h(t,x,y)) \cdot \mathbf{n}_{e,R}\, v_h(x,y) d\,\Gamma(x,y)$$

$$- \int_R \mathbf{F}^{\{k\}}(\mathbf{u}_h(t,x,y)) \cdot \nabla v_h(x,y) dx\, dy$$

$$= \int_R \mathbf{R}^{\{k\}}(\mathbf{u}_h(t,x,y))\, v_h(x,y) dx\, dy,\ \forall v_h \in V_h, \tag{23}$$

where $\mathbf{n}_{e,R}$ is the outward unit normal to the edge e. Notice that $\mathbf{F} \cdot \mathbf{n} = \mathbf{f_x n_x} + \mathbf{f_y n_y}$ is a four-dimensional vector whose k-th component is $\mathbf{F^{(k)}} \cdot \mathbf{n} = \mathbf{f_x}^{(k)} \mathbf{n_x} + \mathbf{f_y}^{(k)} \mathbf{n_y}$. Notice also that $\mathbf{F}(\mathbf{u}_h(t,x,y)) \cdot \mathbf{n}_{e,R}$ does not have a precise meaning, since $\mathbf{u}_h$ is discontinuous at $(x,y) \in e \in \partial R$. Thus, we replace $\mathbf{F}(\mathbf{u}_h(t,x,y)) \cdot \mathbf{n}_{e,R}$ by a suitably chosen numerical flux $\mathbf{h}_{e,R}$, which depends on the two values of $\mathbf{u}_h$ on the edge e. The choice of this numerical flux is crucial since it is through the use of the numerical flux that the upwinding (or the artificial viscosity) which renders the method stable (without destroying its high-order accuracy) is introduced. In this paper, we choose the so-called local Lax-Friedrichs flux. Finally, we replace the integrals above by quadrature rules to obtain the discrete equations. In this way, we obtain a weak formulation which defines the operators $\mathbf{L}_h$ and $\mathbf{R}_h$.

3.3 The Local Projection $\Lambda \Pi_h$

The local projection (limiter) is devised to prevent the appearance of spurious oscillations in the approximate solution. The local averages are unchanged

to preserve the conservativity of the method, but the local variations in the x-direction and in the y-direction must be controlled to avoid the unphysical oscillations. One can alternatively take into account the local characteristic directions along which information travels with different speeds. Taking these characteristic directions into account results in a better control of the oscillations and in a higher quality of the approximation.

3.4   The Right-Hand Side $\mathbf{R}(\mathbf{u}_h)$

In this section we show how to evaluate the function $\mathbf{R}(\mathbf{u_h}) = \xi_{\mathbf{E}}(\mathbf{u_h}) + \xi_c(\mathbf{u_h}) + \xi_{heat}(\mathbf{u_h})$ for a given $\mathbf{u_h}$.

To evaluate $\xi_c(\mathbf{u_h})$, we simply use the equations (9–10) and (4–5). To evaluate $\xi_{\mathbf{E}}(\mathbf{u_h})$, we need a numerical method to obtain an approximation $\mathbf{E}_h$ to the electric field $\mathbf{E}$. The equations defining the electric field are the equations (7–8) and some boundary conditions we write as follows:

$$\phi = \phi_D, \qquad \text{on } \partial\Omega_D, \tag{24}$$

$$\mathbf{E} \cdot \mathbf{n} = \mathbf{0}, \qquad \text{on } \partial\Omega_N, \tag{25}$$

where $\partial\Omega = \partial\Omega_D \cup \partial\Omega_N$ and $\partial\Omega_D \cap \partial\Omega_N = \emptyset$. We discretize these equations with the lowest-order Raviart-Thomas mixed method which defines the approximation $(\mathbf{E}_h, \phi_h) \in \mathbf{U_h} \times \mathbf{W_h}$ as the solution of the following weak formulation:

$$(\nabla \cdot \mathbf{E}_h, w) = \left(\frac{e}{\epsilon}(n_d - n_h), w \right), \forall w \in W_h, \tag{26}$$

$$(\mathbf{E}_h, \mathbf{v}) - (\phi_h, \nabla \cdot \mathbf{v}) = -\langle \phi_D, \mathbf{v} \cdot \mathbf{n} \rangle_{\partial\Omega_D}, \forall \mathbf{v} \in \mathbf{U}_h, \tag{27}$$

where n_h is the approximate density given by the RKDG method, and

$$\mathbf{U}_h = \left\{ \mathbf{v} \in \mathbf{H}(\nabla \cdot; \Omega) : \mathbf{v}|_R = (a_R^1 + a_R^2 x, a_R^3 + a_R^4 y) \right\},$$

$$a_R^i \in \mathbb{R}, \ \forall R \in \mathcal{T}_h; \mathbf{v} \cdot \mathbf{n}|_{\partial\Omega_N} = 0, \tag{28}$$

$$W_h = \left\{ w \in L^2(\Omega) : w|_R \quad \text{is a constant}, \ \forall R \in \mathcal{T}_h \right\}. \tag{29}$$

It can be shown that the above system has a unique solution in $\mathbf{U_h} \times \mathbf{W_h}$ whose approximation of the electric field is second-order accurate. We use Lagrange multipliers, which render the matrix of the resulting method a symmetric positive definite matrix. We invert it by using the conjugate gradient method with incomplete Choleski factorization as preconditioner. To evaluate $\xi_{heat}(\mathbf{u_h})$ we also use the Raviart-Thomas spaces; the procedure is analogous.

We remark that the procedure used here for evaluating the second derivative terms in $\xi_{heat}(\mathbf{u_h})$ is efficient only for the second order schemes, due to mass lumping. A more general approach which keeps the local property of the discontinuous Galerkin method and works for arbitrarily high order of accuracy is the local discontinuous Galerkin method in [7].

4 The Simulation of the MESFET

4.1 Basic MESFET Description

Next we describe a two dimensional MESFET of the size $0.6 \times 0.2 \mu m^2$. The source and the drain each occupies $0.1\mu m$ at the upper left and the upper right, respectively, with a gate occupying $0.2\mu m$ at the upper middle (Fig. 1). The doping is defined by $n_d = 3 \times 10^5 \mu m^{-3}$ in $[0, 0.1] \times [0.15, 0.2]$ and in $[0.5, 0.6] \times [0.15, 0.2]$, and $n_d = 1 \times 10^5 \mu m^{-3}$ elsewhere. We apply, at the drain, voltage biases varying up to $vbias = 2$V. This bias has been described in [3] as a symmetry breaking parameter for the concentration and velocity, with respect to the center of the gate. The gate is a Schottky contact, with negative voltage bias up to $vgate = -0.8$V and very low concentration value $n = 3.8503 \times 10^{-8} \mu m^{-3}$ (following Selberherr [12]). The lattice temperature is taken as $T_0 = 300$ K. The mathematical model for the MESFET is the system (1–3), coupled to Poisson's electrostatic equation (7–8).
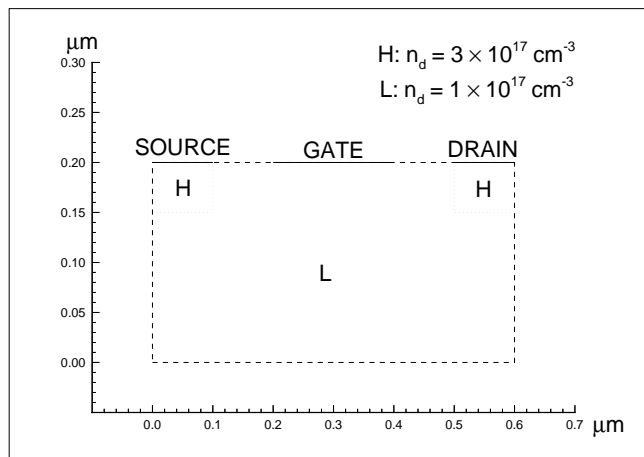

Fig. 1. Two dimensional MESFET. The geometry and the doping n_d.

4.2 Characteristics

We display the concentration, n, in Fig. 2 below, as well as the tangential velocity component, v_x, in Fig. 3 below, obtained from the discontinuous Galerkin method described above. Uniform rectangular meshes of 96×32 and 192×64 were employed for the simulations in which the method is run until the steady state is reached. The results shown are those obtained with the 192×64 mesh. The boundary conditions are determined as follows.

(i) At the source, gate, and drain: $n = n_d$, $v_x = 0 \, \mu m/ps$.
(ii) At all other parts of the boundary: Homogeneous Neumann conditions are imposed.
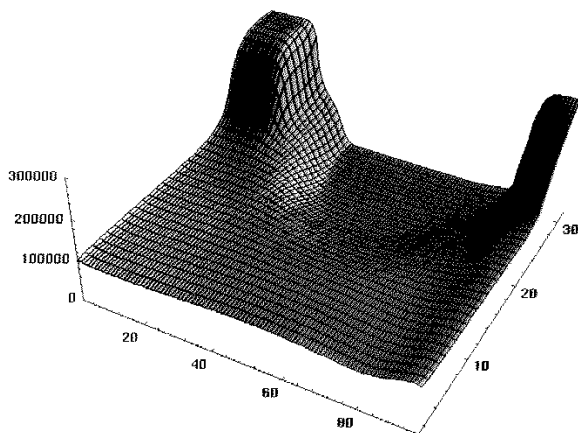

Fig. 2. Concentration n, per μ^3. Domain slightly rotated clockwise from Fig. 1. Axis units defined by (2) grid points per unit.

Notice the boundary layer for n at the drain, but not at the source. This is reasonable since the drain is an outflow boundary and the source is an inflow boundary. A rapid drop of n at the depletion region occurs near the gate. The normal velocity component at the gate appears to be negligible, while the horizontal component shows evidence of strong carrier movement toward the source beneath the left gate area, and strong movement toward the drain immediately to the left of the drain junction. Notice the cusps and strong gradients in the components of the velocity.

5 The Quantum Hydrodynamic Model

The quantum hydrodynamic model used in this paper was derived by Gardner in [8]. In this section, we shall review the basic characteristics of the model
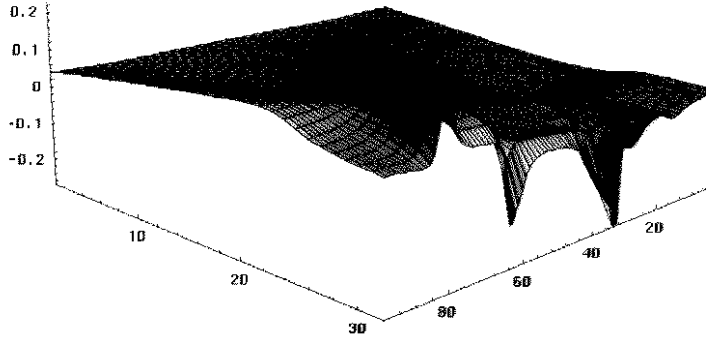
Fig. 3. Horizontal Velocity Component v_x, in μm/ps. See Fig. 2.

as it was described in [5]. An existence theorem for the reduced model was obtained in [15]. The model is also discussed in [9].

The QHD model has exactly the same structure as the classical hydrodynamic model (electrogasdynamics), where we now permit a non-isotropic stress tensor:

$$\frac{\partial n}{\partial t} + \frac{\partial}{\partial x_i}(nv_i) = 0, \tag{30}$$

$$\frac{\partial}{\partial t}(mnv_j) + \frac{\partial}{\partial x_i}(v_i mnv_j - P_{ij}) = -n\frac{\partial V}{\partial x_j} - \frac{mnv_j}{\tau_p} \tag{31}$$

$$\frac{\partial w}{\partial t} + \frac{\partial}{\partial x_i}(v_i w - v_j P_{ij} + q_i) = -nv_i\frac{\partial V}{\partial x_i} - \frac{\left(w - \frac{3}{2}nT_0\right)}{\tau_w} \tag{32}$$

in conjunction with Poisson's equation, (7–8), where P_{ij} is the stress tensor, $V = -e\phi$ is the potential energy, T_0 is the temperature of the semiconductor lattice in energy units (k is set equal to 1), Spatial indices i, j equal 1, 2, 3, and repeated indices are summed over. T is the electron temperature in energy units.

Quantum mechanical effects appear in the stress tensor and the energy density. Gardner derived the stress tensor and the energy density based upon the $O(\hbar^2)$ momentum-shifted thermal equilibrium Wigner distribution function:

$$P_{ij} = -nT\delta_{ij} + \frac{\hbar^2 n}{12m}\frac{\partial^2}{\partial x_i \partial x_j}\log(n) + O(\hbar^4) \tag{33}$$

$$w = \frac{3}{2}nT + \frac{1}{2}mnu^2 - \frac{\hbar^2 n}{24m}\nabla^2\log(n) + O(\hbar^4). \tag{34}$$

In one dimension, the QHD model requires eight boundary conditions. Well-posed boundary conditions for the resonant tunneling diode are $n = n_d$,

$\partial n/\partial x = 0$, and $\partial T/\partial x = 0$ at the left and right diode boundaries x_L and x_R, with a bias ΔV across the device: $V(x_L) = T \log(n/n_i)$ and $V(x_R) = T \log(n/n_i) + e\Delta V$, where n_i is the intrinsic electron concentration.

To exhibit hysteresis, we simulate a GaAs resonant tunneling diode with double $Al_{0.3}Ga_{0.7}As$ barriers (the barrier height $\mathcal{B} = 0.209$ eV). The doping density $n_d = 10^{18}$ cm^{-3} in the n^+ source and drain, and $n_d = 5 \times 10^{15}$ cm^{-3} in the n channel. The channel is 250 Å long, the barriers are 50 Å wide, and the well between the barriers is 50 Å wide. The device has 50 Å spacers between the barriers and the contacts (source and drain) to enhance negative differential resistance.

The current-voltage curve for the resonant tunneling diode is plotted in Fig. 4 for ΔV increasing from 0 volts to 0.22 volts (upper curve) and decreasing from 0.22 volts to 0 volts (lower curve). Note that hysteresis occurs predominantly in the region of negative differential resistance. The physical mechanism for hysteresis is that electrons "see" a different potential energy due to different accumulated electron charges in the diode when the applied voltage is decreasing than when the applied voltage is increasing.
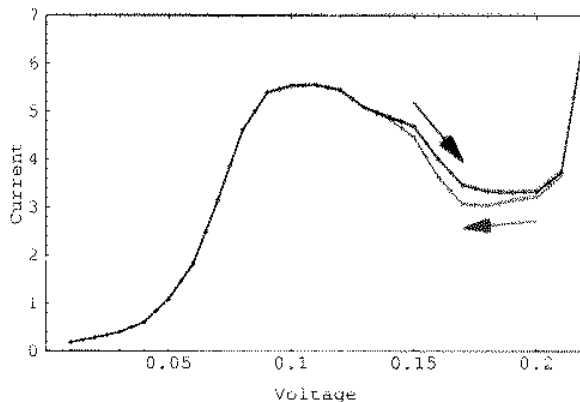

Fig. 4. Current-Voltage Curve.

References

1. Baccarani, G., Wordeman, M.R.: An investigation of steady-state velocity overshoot effects in Si and GaAs devices. Solid State Electr., **28** (1985) 407–416
2. Bløtekjær, K.: Transport equations for electrons in two–valley semiconductors. IEEE Trans. Electron Devices, **17** (1970) 38–47
3. Chen, G.-Q., Jerome, J. W., Shu, C.-W., Wang, D.: Two carrier semiconductor device models with geometric structure and symmetry properties. In: J. Jerome (ed.) *Modelling and Computation for Applications in Mathematics, Science, and Engineering*, Clarendon Press, Oxford 1998, pp. 103–140
4. Chen, Z., Cockburn, B., Jerome, J. W., Shu, C.-W.: Mixed-RKGD finite element methods for the 2-D hydrodynamic model for semiconductor device simulation. VLSI DESIGN **3** (1995) 145–158
5. Chen, Z., Cockburn, B., Gardner, C., Jerome, J. W.: Quantum hydrodynamic simulation of hysteresis in the resonant tunneling diode. J. Comp. Phys. **117** (1995) 274–280
6. Cockburn, B., Hou, S., Shu, C.-W.: TVB Runge-Kutta local projection discontinuous Galerkin finite element method for conservation laws IV: the multidimensional case. Math. Comp. **54** (1990) 545–581
7. Cockburn, B., Shu, C.-W.: The local discontinuous Galerkin method for time-dependent convection-diffusion systems, SIAM J. Numer. Anal. **35** (1998) 2440–2463
8. Gardner, C.L.: The quantum hydrodynamic model for semiconductor devices. SIAM J. Appl. Math. **54** (1994) 409–427
9. Jerome, J. W.: *Analysis of Charge Transport: A Mathematical Study of Semiconductor Devices.* Springer-Verlag, Heidelberg, 1996
10. Jerome, J. W., Shu, C.-W.: Energy models for one-carrier transport in semiconductor devices. In: W.M. Coughran. J. Cole, P. Lloyd, and J.K. White (eds.) *Semiconductors, Part II. IMA Volumes in Mathematics and Its Applications*, vol. 59. Springer, New York 1994, pp. 185–207
11. Jerome, J. W., Shu, C.-W.: Transport effects & characteristic modes in the modeling & simulation of submicron devices. IEEE Trans. on Computer–Aided Design. **14** (1995) 917–923
12. Selberherr, S.: *Analysis and Simulation of Semiconductor Devices.* Springer-Verlag, Wien-New York, 1984
13. Shu, C.-W., Osher, S.J.: Efficient implementation of essentially non-oscillatory shock capturing schemes. J. Comp. Phys. **77** (1988) 439–471
14. Shu, C.-W., Osher, S.J.: Efficient implementation of essentially non-oscillatory shock capturing schemes, II. J. Comp. Phys. **83** (1989) 32–78
15. Zhang, B., Jerome, J. W.: On a steady-state quantum hydrodynamic model for semiconductors. Nonlinear Anal. **26** (1996) 845–856